An Investigation of the Rotamers of Butadiene by High-Resolution Infrared Spectroscopy

Norman C. Craig*,† and Robert L. Sams‡

Department of Chemistry and Biochemistry, Oberlin College, Oberlin, Ohio 44074, and Environmental and Molecular Sciences Laboratory, Pacific Northwest National Laboratory, P.O. Box 999, Mail Stop K8-88, Richland, Washington 99352

Received: August 28, 2008; Revised Manuscript Received: October 16, 2008

A wide-ranging investigation of high-resolution infrared spectra of 1,3-butadiene was undertaken with the prime objective of finding subbands in the rotational structure attributable to the gauche rotamer, from which information about the molecular structure could be derived. A weak band near 750 cm^{-1}, which had previously been assigned to the gauche rotamer, has been shown to be a difference band for the trans rotamer. In support of the analysis of this band, the rotational structure, including two hot bands, was analyzed in the C-type band for the $\nu_{12}(a_u)$ mode near 525 cm^{-1} and in the C-type band near 162 cm^{-1} for the $\nu_{13}(a_u)$ mode. An unsuccessful attempt was made to extend the analysis of the B-type component of the A/B-type band for $\nu_{17}(b_u)$ near 3000 cm^{-1}. With the exception of the two weak Q branches at 463.82 and 462.16 cm^{-1}, no new evidence for the gauche rotamer in the gas phase was found.

1. Introduction

The principal rotamer of 1,3-butadiene at room temperature is the planar, *s*-trans form. A higher energy, nonplanar gauche form also exists in the gas phase. Evidence for the gauche rotamer or the possible variant in condensed phases, the planar *s*-cis rotamer, has been obtained experimentally and through quantum chemical (QC) calculations. Initially, the most extensive experimental evidence for the gauche or cis rotamer came from the matrix-isolation studies of Squillacote et al.[1] and of Huber-Wälchli and Günthard.[2] A beam of a dilute mixture of butadiene and argon, heated to temperatures as high as 850 °C, was sprayed onto a crystal window mounted in a cryostat cooled to 30 K[1] or to liquid helium temperature,[2] and the infrared spectrum was recorded. A number of peaks, which were assigned to the cis or gauche rotamer, grew in as the temperature of the beam was raised. These investigations of the infrared spectra of matrix-isolated material have been confirmed and extended to Raman spectroscopy by Furukawa et al.[3] and Michl et al.[4–6] For condensed phases, Michl and co-workers concluded that the evidence for the distinction was uncertain between the gauche and trans species, which differ by no more than 4.5 kJ/mol.[6]

In addition, in their infrared investigation, Squillacote et al. showed that the trans and gauche or cis rotamers in the matrix phase differed in the maximum for UV absorption and could be interconverted with selected UV radiation.[1] The maximum for absorption by the trans rotamer was 212 nm, and the maximum for the cis or gauche rotamer was 226 nm. Saltiel et al. recorded ultraviolet spectra of butadiene in the gas phase from 5 to 93 °C.[7] From the deconvoluted spectra as a function of temperature, they obtained a higher energy ($\Delta_r H°_{320}$) of 12.24 kJ/mol for the gauche rotamer and a concentration of about 5% for this rotamer at room temperature. They reported UV maxima of 209 and 215 nm respectively for the trans and gauche rotamers in the gas phase. The decidedly lower maximum for absorption by the gauche rotamer compared with the observations by Squillacote et al.[1] in an argon matrix is consistent with the occurrence of the gauche rotamer in the gas phase and the cis rotamer in condensed phases. The planar cis rotamer is expected to have its UV maximum at a longer wavelength because of greater π-electron delocalization. Mui and Grunwald also studied the temperature dependence of the UV absorption of butadiene in the gas phase between 298 and 621 K in the region where only the cis/gauche rotamer absorbs. They found 12.6 kJ/mol for $\Delta H°_{520}$.[8]

Evidence for the gauche rotamer in the gas phase seemed to be reinforced by the work of Engeln et al.[9] They studied the gas-phase Raman spectrum of the hot band transitions of the overtone of the torsional mode of the trans rotamer and also reported similar transitions of the gauche rotamer. This work built on earlier studies by Carriera[10] and Durig et al.[11] Panchenko et al. reported a Raman investigation of two deuterium isotopomers of butadiene, but they made no assignments for the gauche rotamer.[12] A sufficient number of transitions in the vibrational spectrum of butadiene was observed by Engeln et al. to yield a torsional potential function connecting the trans, gauche, and cis rotamers.[10] The barrier between the trans and gauche rotamers was 25 kJ/mol (78° torsion angle from the trans rotamer), and the gauche rotamer was 12 kJ/mol above the trans rotamer (38° torsion angle from the cis rotamer). The cis rotamer was at a transition state approximately 4.5 kJ/mol above the gauche rotamer. In earlier work, Panchenko et al. used theory and experiment to come to a similar conclusion.[13]

Recent calculations by Karpfen and Parasuk at a high level of theory indicate that the cis-gauche energy difference may be as low as 2.4 kJ/mol.[14] Murcko et al. also found a small value for this energy difference in lower level theoretical calculations.[15] Thus, the assignments of features in the Raman spectrum to the gauche rotamer in the low-frequency region, from which the higher barrier was derived, must now be regarded as uncertain.[9] More doubts about the assignments for the gauche rotamer in the gas-phase Raman spectrum come from other considerations. The intensity of the keystone band at 269.9 cm^{-1} assigned to the 2−0 transition of ν_{13}, the torsional mode of the gauche rotamer, seems much too high for an overtone, as noted

* Correspond author.
† Oberlin College.
‡ Pacific Northwest National Laboratory.

10.1021/jp807677y CCC: $40.75
Published on Web 11/14/2008

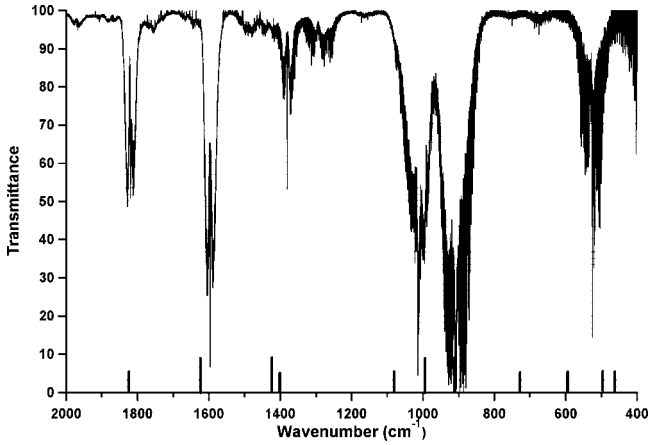

Figure 1. Midinfrared spectrum of butadiene in the gas phase with bars showing bands attributed to the gauche/cis rotamer in matrix spectra[1,2] (pressure 32 Torr and resolution 0.1 cm^{-1}).

by Engeln et al.[9] New predictions place the ν_{12} fundamental at 275 cm^{-1} and give it significant Raman activity.[16,17] This fundamental is a more likely assignment for the band at 269.9 cm^{-1}.

In addition to the Michl group,[6] other groups have used QC calculations to predict the structure and vibration frequencies of the gauche and cis rotamers of butadiene. Wiberg and co-workers,[15,18] Panchenko and co-workers,[19−21] and Tang and Bally have done so.[22] The conclusion from all of these calculations is that various wavenumbers for the gauche and cis rotamers differ no more than 20 cm^{-1} with the exception of 26, 36, and 43 cm^{-1}.[6] Of course, the selection rules differ between the gauche rotamer with C_2 symmetry and the cis rotamer with C_{2v} symmetry.

Structural evidence for the gauche rotamer has been sought in gas-phase investigations. Published reports tell of unsuccessful microwave searches for rotational transitions of the gauche rotamer,[23,24] which has a small dipole moment (B3LYP/aug-cc-pVTZ estimate of 0.10 D) in addition to being a minor component at room temperature. A promising report of structural information was the infrared investigation of the rotational structure in the weak band located near 750 cm^{-1}, which was assigned to the gauche rotamer. DeMaré et al. found Q-branch structure for subbands of a B-type band at moderate resolution.[20] Though a bit small, this Q-branch spacing was in reasonable agreement with the predictions for the structure of the gauche rotamer and unsuited to the trans rotamer.

For the present study, we intended to reinvestigate the rotational structure in the band near 750 cm^{-1} with much higher resolution infrared spectroscopy and obtain structural information from its *A*, *B*, and *C* rotational constants. We also planned to investigate other regions of the spectrum with high resolution. As a prelude, the gas phase spectrum of BDE was observed at 0 and 50 °C. Regions where relative intensities increased with temperature became targets for careful investigation. These regions were close to those for which bands had been observed for the gauche/cis species in matrices. Figure 1 shows the location of bands, as bars at the bottom of the spectrum, from the matrix spectra along with bands from the gas phase spectrum.[1,2] Although the gauche/cis band near 730 cm^{-1} is in an open region, the other promising bands fall in the wings of bands of the trans rotamer in the gas phase. The band located near 600 cm^{-1} is the most distant from the center of a band of the trans rotamer. In this case, the neighboring trans rotamer band is at 525 cm^{-1}. Another promising region is near 465 cm^{-1}.

The weak band in the gas-phase spectrum near 750 cm^{-1} has now, regrettably, been reassigned as a difference band of the abundant trans rotamer. To make this reassignment with confidence, it was necessary to investigate hot band series in other bands of the trans rotamer. In the first instance, these hot bands, which arise from thermal excitations of the torsional mode $\nu_{13}(a_u)$, were observed in the C-type band for $\nu_{12}(a_u)$ near 525 cm^{-1}. As confirmation, corresponding hot bands were assigned in the C-type band for the ν_{13} itself near 162 cm^{-1}. Detailed analysis of the rotational structure of the band centered near 525 cm^{-1} was also essential as a prelude to the search in its wings for subbands of the gauche rotamer. We have also studied the spectrum in the CH stretching region, where Halonen et al. have recently reported a high-resolution laser investigation with jet-beam cooling.[25] From their introduction, it seems that they also sought spectral evidence for the gauche rotamer in the gas phase. The present high-resolution work for the trans rotamer of butadiene extends our previous work on the analysis of bands for $\nu_{20}(b_u)$ at 1596.446 cm^{-1} (A-type) and for $\nu_{11}(a_u)$ at 908.072 cm^{-1} (C-type) of this rotamer.[26]

2. Experimental Section

The butadiene, supplied by Matheson, was of research purity (99.8% with a trace of CO_2). Samples were held in a multipass White cell at 21 °C, and all but the lowest frequency spectrum were recorded with a Bruker IFS 120 HR at PNNL. The lowest frequency spectrum was recorded on a Bruker 125 instrument. Details of the use of this instrumentation at PNNL have been reported.[27] Table 1 gives the conditions for the various spectra.

The moderate resolution gas-phase spectrum in Figure 1 was recorded on a Nicolet 760 Magna FT spectrometer with a KBr beamsplitter and a DTGS detector at 0.1 cm^{-1} resolution. The spectrometer was purged with dry nitrogen. The gas cell had an internal length of 10 cm and KBr windows.

The Loomis-Wood (LW) pattern-recognition program, written at Justus Liebig Universität in Giessen, Germany, was employed for finding and assigning the rotational lines contributing to the complex spectra.[31] We applied the bootstrap strategy for identifying the subband series that has been described in detail before.[32] A Watson-type Hamiltonian in the asymmetric top reduction and the I^r representation[33] was used to fit the rotational transitions by a modified version of Dr. Arthur Maki's ASYM program, written in Fortran. In fitting ground state combination differences (GSCDs) and lower state combination differences (LSCDs) care was taken to avoid redundant use of experimental data caused by alternative loops.

3. Results and Discussion

3.1. General Considerations. The trans rotamer of 1,3-butadiene is centrosymmetric and a near-prolate top with C_{2h} symmetry. The nine modes of the a_g symmetry species and the three modes of the b_g symmetry species are inactive in the infrared spectrum. The four modes of the a_u symmetry species have dipole moment changes along the *c* principal rotation axis, which is out of plane, and thus have C-type band shapes in the gas-phase infrared spectrum. C-type selection rules for rotational transitions are $\Delta J = 0, \pm1$, $\Delta K_a = \pm1$, and $\Delta K_c = 0, \pm2$. The eight modes of the b_u symmetry species have, in principle, changing dipole moment components along both the *a* and *b* principal rotation axes. Thus, the band shapes in the gas-phase infrared spectrum for these modes are hybrid A/B-bands. A-type selection rules for rotational transitions are $\Delta J = 0, \pm1$, $\Delta K_a = 0$, and $\Delta K_c = \pm1, \pm3$; B-type selection rules are $\Delta J = 0, \pm1$, $\Delta K_a = \pm1$, and $\Delta K_c = \pm1, \pm3$.

TABLE 1: Experimental Conditions for Spectra

region/cm^{-1}	resolution/ cm^{-1}	beam-splitter	detector	no. of scans	path length/m	pressure/ Torr	calibrant gas
2800−200	0.003	CaF_2	InSb	512	16	0.4	OCS[a]
610−806	0.002	KBr	HgCdTe[b]	512	32	5	CO_2[c]
440−647	0.0015	KBr	Si:Ga[d]	512	3.2	0.64	CO_2[c]
410−660	0.0025	KBr	Si[f]	40	32	3.6	CO_2[c]
50−352	0.0018	Mylar	Si[f]	40	19.2	3.0	H_2O

[a] Reference 28. [b] Liquid nitrogen temperature. [c] Reference 29. [d] Liquid helium temperature. [e] Bolometer; liquid helium temperature. [f] Reference 30.

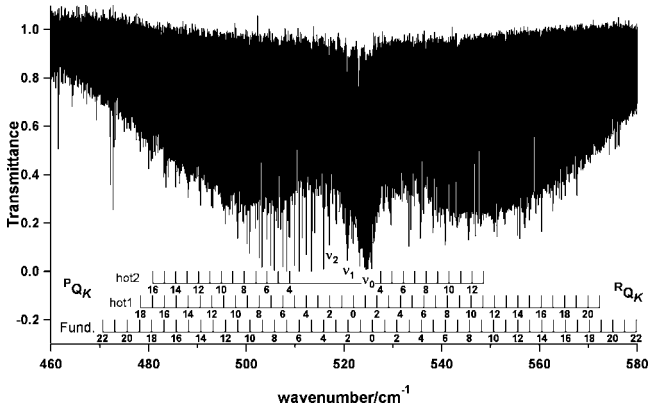

Figure 2. Overall view of the high-resolution scan of the C-type band at 525 cm^{-1} for ν_{12} of the trans rotamer at 0.64 Torr (2.06 Torr m).

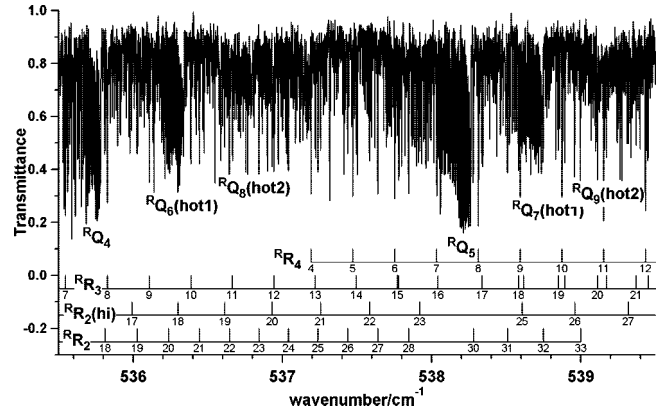

Figure 3. An example of the details of the assignments in the R branch of the C-type band of the trans rotamer at 525 cm^{-1}.

In new calculations, the gauche rotamer of 1,3-butadiene is predicted to have a dihedral angle of 35.5° relative to the planar cis configuration. *gauche*-Butadiene approaches a prolate symmetric top with a calculated kappa of −0.8707 [CCSD(T)/aug-cc-pVNZ model with extrapolation to a complete basis set and corrections for frozen core electrons and relativity].[34] The equilibrium rotational constants predicted by these calculations are $A = 0.71195$, $B = 0.19033$, and $C = 0.15428$ cm^{-1}. B_{av}'' $[(B'' + C'')/2]$ is 0.1723 cm^{-1}. The gauche rotamer has only C_2 symmetry, and all modes are infrared active. Because the *b* principal rotation axis coincides with the C_2 symmetry axis, the fully symmetric modes have B-type band shapes in the gas-phase infrared spectrum and B-type selection rules for rotational transitions. The other modes have hybrid A/C-type band shapes and corresponding selection rules for rotational transitions.

3.2. Analysis of Rotational Structure in the C-type Band Near 525 cm^{-1}. Analyses have been performed of the rotational structure accompanying the transitions from the ground state and from the strongest hot bands for the C-type band at 525 cm^{-1}. These transitions are based on $\nu_{12}(a_u)$, which is largely out-of-plane CH_2 twisting. The hot band transitions arise from excited states of the $\nu_{13}(a_u)$ torsional mode at 162 cm^{-1}. A moderate intensity scan (0.64 Torr, 2.06 Torr m) was used for this investigation to permit a full analysis of the band center. Figure 2 shows the overall structure of the band at 525 cm^{-1} with combs marking the subband Q branches of transitions from the ground state and the two hot bands. As an example of the assignments of the fundamental, the details of the $^{R}R_K$ series in the vicinity of $^{R}Q_4$ and $^{R}Q_5$ are displayed in Figure 3. Hot band Q branches are designated in this figure as "hot1" and "hot2" for the first and second hot bands.

The results of fitting rotational structure for the fundamental to Watson-type Hamiltonians are given in Table 2. A full set of quartic centrifugal distortion constants and two sextic centrifugal distortion constants have been determined for the ground state (GS) and the upper state (US) of the ν_{12} fundamental. The ground state rotational constants given in column one in this table came from a composite fit of GSCDs arising from the band for $\nu_{11}(a_u)$ analyzed in our earlier work[26] and the ν_{12} band in this present work. Only GSCDs (1301) from the center of the ν_{11} band out to $^{R}R_{13}/^{P}P_{15}$ were included in the data set because of the limitation to 3000 transitions in our version of ASYM. GSCDs contributions from the C-type band at 525 cm^{-1} came from lines with K_a up to 21 and J up to 68 for a total of 1689. Rotational constants for the US of the fundamental are in column two of Table 2. For the ν_{12} fundamental, a perturbation beginning at $K_a' = 17$ limited the fitting of US rotational constants to 2838 transitions. These transitions came from subbands $^{P}Q_5$ through $^{R}Q_5$ and $^{P}P_{18}$ through $^{R}R_{16}$, as well as the offside series $^{P}R_1$ and $^{R}P_0$. Asymmetry splitting was assigned as far out as $K_a' = 8$, and J values ranged up to 71. The band center is 524.5739 cm^{-1}. Supplementary tables give details of the assignments. Table S1 in the Supporting Information gives the full set (from ν_{11} and ν_{12}) of GSCDs in the fit of GS rotational constants. Table S2 in the Supporting Information gives the lines in subbands up to $K_a' = 16$ and the fit to US rotational constants for the ν_{12} fundamental. The remaining $^{P}P_K$ and $^{R}R_K$ series for $K_a' = 17$ to 21 for the ν_{12} fundamental are an addendum to Table S2 in the Supporting Information.

A full range of subband series of the first hot band for ν_{12}, which arises from the thermal excitation of one quantum in the torsional mode ν_{13} at 162 cm^{-1}, were assigned. LSCDs of the hot band were derived from the assignments and were used to fit lower state (LS) rotational constants for this hot band. The fit of the LSCDs was limited to $K_a' \leq 10$ because of a perturbation. The rotational constants for the LS of the first hot band are given in column three in Table 2 under the heading $(\nu_{12} + \nu_{13}) - \nu_{13}$. As seen later in the section on the analysis of the C-type band of the torsional mode, these LS rotational constants are in satisfactory agreement with the rotational constants found for the first excited state of the torsion. With the LS rotational constants held fixed for the first hot band of

TABLE 2: Ground State Rotational Constants and Other Rotational Constants Associated with the ν_{12} Mode of Butadiene

			$(\nu_{12} + \nu_{13}) - \nu_{13}$		$(\nu_{12} + 2\nu_{13}) - 2\nu_{13}$	
	GS[a,b]	ν_{12}[a,c]	LS[a,c]	US[a,e]	LS[a,f]	US[a,g]
A (cm^{-1})	1.3903838(7)	1.3890163(4)	1.344822(3)	1.344379(1)	1.30445(1)	1.30455(1)
B (cm^{-1})	0.1478858(1)	0.14774729(3)	0.147957(1)	0.1478238(1)	0.14814(3)	0.14802(1)
C (cm^{-1})	0.1336939(2)	0.13370760(3)	0.134112(1)	0.1341330(1)	0.13442(2)	0.13444(1)
$10^9\delta_J$ (cm^{-1})	3.585(9)	3.564(7)	3.74(12)	3.74(2)	3.74[h]	3.74[h]
$10^7\delta_K$ (cm^{-1})	1.34(2)	1.32(2)	−1.49(30)	−1.41(7)	−1.41[h]	−1.41[h]
$10^6\Delta_K$ (cm^{-1})	7.318(3)	7.074(3)	−5.07(2)	−4.80(1)	−12.23(8)	−12.6(4)
$10^7\Delta_{JK}$ (cm^{-1})	−2.443(5)	−2.558(2)	−2.45(3)	−2.481(4)	−2.05(28)	−1.96(5)
$10^8\Delta_J$ (cm^{-1})	2.923(4)	2.9311(8)	2.86(4)	2.864(3)	1.91(30)	1.85(2)
$10^{11}\Phi_K$ (cm^{-1})	7.2(4)	−1.8(8)				
$10^{11}\Phi_{KJ}$ (cm^{-1})	−9.4(9)	−7.7(6)				
ν_0 (cm^{-1})		524.573925(9)		520.71038(2)		516.9861(3)
$\Delta\nu_{rms}$ (cm^{-1})	0.000245	0.000182	0.000400	0.000300	0.000544	0.000449
κ	−0.977414	−0.977631	−0.977129	−0.977375	−0.976546	−0.976786
no. of transitions	2990	2838	576	1321	109	287
max K_a'	21	17	10	10	11	11
max J	66	68	47	53	37	47

[a] Uncertainty (1σ) in the last places in the fit in parentheses. [b] Fit to pooled GSCDs: 56.5% from the 525 cm^{-1} band and 43.5% from the 908 cm^{-1} band, which was truncated at $^{R}R_{13}/^{P}P_{15}$ to keep the data set below the limit of 3000 transitions for the program. [c] Fit to GSCDs and the lines for the fundamental of ν_{12}. [d] Fit to LSCDs for the first hot band of ν_{12}. [e] Fit to the LS constants and the lines of the first hot band. [f] Fit to the LSCDs for the second hot band of ν_{12}. [g] Fit to the LS constants and the lines for the second hot band. [h] Transferred from the US constants of the first hot band.

ν_{12}, a fit of the US rotational constants of this band was made to 1321 lines for subband series up to $K_a' = 10$. The results of this fit are given in the fourth column of Table 2. The center of the first hot band is 520.7104 cm^{-1}. Table S3 in the Supporting Information gives the LSCDs and details for the fitting of the LS rotational constants for the first hot band of ν_{12}. We will return to a more accurate fit for the US constants after reporting in the next section on the related analysis of ν_{13} fundamental and its hot bands.

The analysis of the rotational structure associated with the second hot band of ν_{12} proceeded in a similar manner as that for the first hot band. However, the analysis for this band was less complete owing to its weaker intensity and the band center of the fundamental overshadowing low K_a subbands of the R branch from the second hot band. Thus, the analysis of the second hot band lacks subbands with low K_a values, including the central Q branch. In columns five and six in Table 2 under the heading $(\nu_{12} + 2\nu_{13}) - 2\nu_{13}$ are the LS and US rotational constants fitted to the second hot band of ν_{12}. Because of perturbations as well as the limited data set, the LS constants come from fitting only 109 transitions and thus are only approximately determined. This uncertainly affects the US constants as well. Nonetheless, agreement of the LS rotational constants for this hot band with the rotational constants found for the second excited state of ν_{13}, as reported in the next section, is satisfactory and in full support of the interpretation of the second hot band. Table S4 in the Supporting Information contains the LSCDs and the details of fitting rotational constants for the second hot band. We will return to a superior fit for the US of the second hot band after the report on the analysis of the bands associated with ν_{13}.

Figure 4 is an energy level diagram for ν_{12}, ν_{13}, and ν_{15} and combined states. This diagram shows most of the transitions investigated for this paper. Arrows involving ν_{12} and $\nu_{12} + \nu_{13}$ show transitions observed in association with the ν_{12} fundamental. Also shown in Figure 4 are the transitions observed in association with the ν_{13} fundamental and the difference band involving ν_{13} and ν_{15}.

3.3. Analysis of the Rotational Structure in the C-Type Band Near 162 cm^{-1}. After the investigation of the C-type band at 525 cm^{-1} and the use of the LSCDs of the first hot band in the analysis of the difference band near 746 cm^{-1} (vide infra), we investigated the band for the torsional mode near 162 cm^{-1} at 3.0 Torr (58.4 Torr m). Doing so gave direct evidence for the excited states of the ν_{13} mode, despite the challenge of obtaining a good spectrum of a weak band in this difficult spectral region. In Figure 4, the arrows in the stack for ν_{13} show the transitions investigated for this mode.

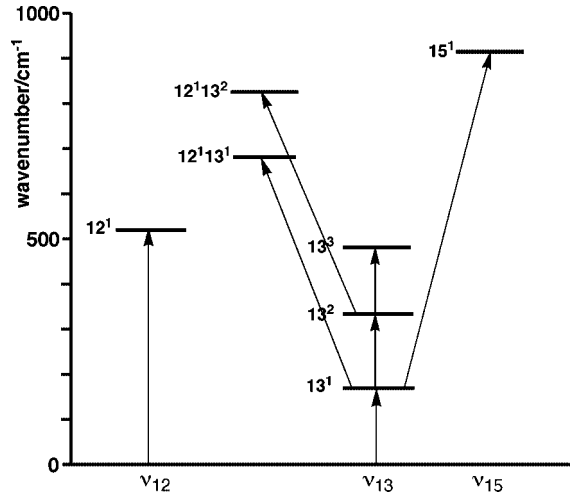

Figure 4. Energy diagram for transitions investigated in association with the ν_{12}, ν_{13}, and ν_{15} fundamentals of the trans rotamer of butadiene.

Figure 5 shows the overall structure of this band from the high-resolution investigation of the band at 162 cm^{-1}. Combs for assignments of subband centers are displayed for the fundamental and the first two hot bands. All of the narrow, intense features in the spectrum came from residual water in the spectrometer. Figure 6 presents details of the assignments of this band in the region of $^{P}Q_7-^{P}Q_9$. Rotational structure for all three bands has been assigned in detail. Upper state combination differences (USCDs) for the first hot band, which are LSCDs for the second hot band, were quite helpful in assigning correct K_a'' values in the R and P branches in the second hot band.

We attempted to find rotational structure for the third hot band, which, based on the Boltzmann population of the third

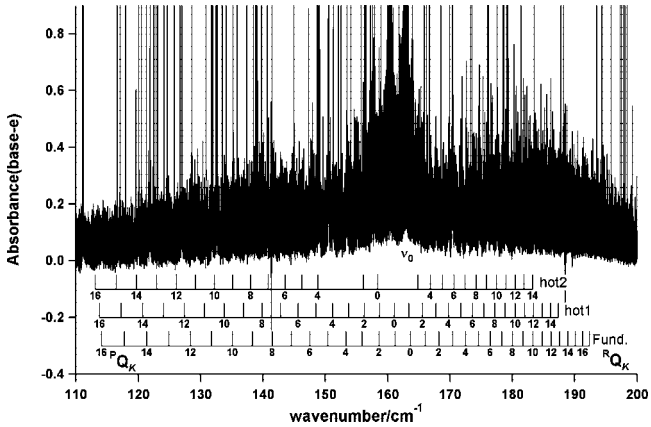

Figure 5. Overall view of the high-resolution scan of the C-type band at 162 cm^{-1} for ν_{13} of the trans rotamer at 3.0 Torr (58.4 Torr m).

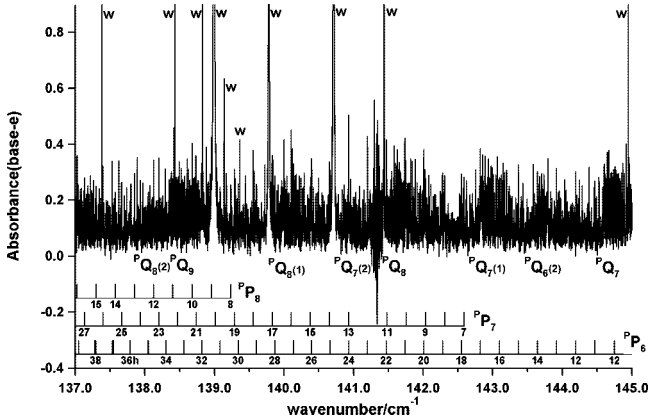

Figure 6. An example of the detail of the assignments in the P branch of the C-type band of the trans rotamer at 162 cm^{-1}.

excited state, is approximately 50% less intense than the second hot band. Our strategy was to suppress the subbands for the fundamental and the first hot band in the Loomis−Wood display. The subbands for the second hot band were left for displaying in different colors to guide the search for subbands from the third hot band. Although a few, tentative assignments for subbands of the third hot band were found, these were too scattered to permit assignment of K_a'' values. Competition of noise with the weak lines of the third hot band interfered with finding the paths of the subband series. In addition, the suppression of lines from the fundamental and the first hot band removed lines from the screen that were at intersections with possible paths for subbands from the third hot band. This lack of lines made it harder to recognize paths for subbands of the third hot band.

Table 3 gives the rotational constants obtained from the analysis of the band for the torsional mode ν_{13} and its two hot bands. The first column gives GS constants fit exclusively to 892 GSCDs from the band for the ν_{13} fundamental. These GS constants compare favorably with those fit to the composite set from other bands, as given in column one in Table 2. The ν_{13} GS constants were used in the fit of the US constants, supplied in column two in Table 3, for the first excited state of the torsional mode. Other columns in Table 3 give LS and US rotational constants for the first and second hot bands, as fitted to data for these bands. Of course, columns two and three in Table 3 are for the same state as are columns four and five for another state. Small differences between the pairs of parameters reflect use of different data sets. The rotational constants for the LS of the first hot band of the torsion in column three in Table 3 are in satisfactory agreement with the LS rotational constants fit to the first hot band of ν_{12}, as given in column three in Table 2. Similarly, the LS rotational constants for the second hot band of ν_{13} in column five in Table 3 are in satisfactory agreement with the LS rotational constants of the second hot band of ν_{12}, as reported in column five in Table 2. Table S5 (Supporting Information) contains the GSCDs derived from the ν_{13} fundamental and the details of the fit for the GS rotational constants. Table S6 (Supporting Information) contains the lines for this fundamental and the fitting of the US constants. An addendum to Table S6 (Supporting Information) contains the assigned lines not used in the US fit.

Table 4 gives the best set of rotational constants for the various states of the ν_{13} mode and for the upper states of the hot bands associated with the ν_{12} mode. The constants in this table were obtained by fitting pooled data. Thus, for the rotational constants of the upper state of the fundamental of ν_{13}, the data set consisted of USCDs for the fundamental, LSCDs for the first excited state of the first hot band for ν_{13}, and the LSCDs from the first hot band for ν_{12}. Rotational constants fit to this pool of data are in column one in Table 4. We prefer these rotational constants for the US of the ν_{13} fundamental. Using the rotational constants from column one in Table 4 as LS rotational constants, the US rotational constants for the first hot band were fitted and reported in column two of Table 4. We did an alternative determination of these rotational constants with data pooled from USCDs of the first hot band of ν_{13}, LSCDs from the second hot band of ν_{13}, and LSCDs from the second hot band of ν_{12}. However, this data set consisted of only 608 transitions, and thus the result of the fit was regarded as inferior to that obtained from fitting the 1192 lines in the first hot band of ν_{13}. The results of the fit to this pool of data are not reported here. For the best rotational constants for the third excited state of the ν_{13} mode, which are reported in column three in Table 4, the US rotational constants were fitted to the observed lines of the second hot band and the US rotational constants of the first excited state of ν_{13}, as given in column two of Table 4. Assignments for the $^{R}Q_0$ and $^{P}Q_1$ subbands in the band center of the second hot band reinforced the fit of the rotational constants for the third excited state of the torsional mode. These two subbands do not, however, contribute to an improvement in the LSCDs for the second hot band because they do not form LSCDs with other subbands.

Best values for the US rotational constants for the two hot bands of the ν_{12} mode are reported in columns four $(\nu_{12} + \nu_{13}) - \nu_{13}$ and five $(\nu_{12} + 2\nu_{13}) - 2\nu_{13}$ of Table 4. LS rotational constants for the first hot band were from column one in Table 4, and LS rotational constants for the second hot band were from column two in Table 4. Given the limitations of the LSCDs used in the original fit for the US of the second hot band, the agreement between the values in column four of Table 2 with column four in Table 4 and column six of Table 2 with column five in Table 4 is gratifying.

Supplementary tables give the data sets and fitting details for the results in Table 4. Table S7 (Supporting Information) contains the pooled combination difference data used to obtain the improved fit of rotational constants to the upper state of the fundamental of ν_{13}. Table S8 (Supporting Information) contains the lines used in the improved fit for the US of the first hot band of ν_{13}. Assigned lines not used in the fit are an addendum. Table S9 (Supporting Information) gives the lines used in the improved fit for the US state of the second hot band of ν_{13} with lines unused in the fit given in an addendum. Tables S10 and S11 (Supporting Information) contain lines and the fit of US

TABLE 3: Rotational Constants and Vibrational Frequencies for the Torsional Mode (ν_{13}) of Butadiene.

			$2\nu_{13} - \nu_{13}$		$3\nu_{13} - 2\nu_{13}$	
	GS[a,b]	ν_{13}[a,c]	LS[a,d]	US[a,e]	LS[a,f]	US[a,g]
A (cm^{-1})	1.390377(1)	1.344771(1)	1.344815(4)	1.304294(2)	1.30431(1)	1.268228(3)
B (cm^{-1})	0.1478867(5)	0.1479624(1)	0.147958(1)	0.1480370(1)	0.14802(1)	0.148106(1)
C (cm^{-1})	0.1336940(2)	0.1341189(1)	0.134113(1)	0.1345438(1)	0.13456(1)	0.135005(1)
$10^9\delta_J$ (cm^{-1})	3.82(12)	3.67(2)	3.87(9)	3.76(2)	3.76[h]	3.04(23)
$10^7\delta_K$ (cm^{-1})	1.48(32)	−1.52(7)	−1.65(30)	−3.64(7)	−3.64[h]	−12.9(23)
$10^6\Delta_K$ (cm^{-1})	7.287(4)	−5.48(1)	−5.10(3)	−13.36(2)	−13.10(8)	−18.05(4)
$10^7\Delta_{JK}$ (cm^{-1})	−2.40(1)	−2.442(4)	−2.41(5)	−2.402(7)	−2.56(15)	−2.47(3)
$10^8\Delta_J$ (cm^{-1})	2.91(2)	2.967(3)	2.80(5)	2.865(3)	3.14(11)	3.00(7)
ν_0 (cm^{-1})		162.41947(2)		159.91106(3)		157.25280(6)
$\Delta\nu_{rms}$ (cm^{-1})	0.00038	0.00035	0.00044	0.00034	0.000499	0.000422
κ	−0.977412	−0.977130	−0.977130	−0.976930	−0.976986	−0.976879
no. of transitions	892	1510	493	1174	135	528
max K_a'	17	10	10	9	9	9
max J	53	60	45	50	45	55

[a] Uncertainty (1σ) in the last places in the fit in parentheses. [b] Fit to GSCDs from the fundamental. [c] Fit to GSCDs and the lines for the fundamental of ν_{13}. [d] Fit to LSCDs for the first hot band of ν_{13}. [e] Fit to the LS constants and the lines of the first hot band. [f] Fit to the LSCDs for the second hot band of ν_{13}. [g] Fit to the LS constants and the lines for the second hot band. [h] Transferred from the US constants in column 4 for the first hot band.

TABLE 4: Best Rotational Constants of $n\nu_{13}$ and $(\nu_{12} + n\nu_{13}) - n\nu_{13}$ States of Butadiene from Pooled Data

	ν_{13}[a,b]	$2\nu_{13}$[a,c]	$3\nu_{13}$[a,d]	$(\nu_{12}+\nu_{13})$ - ν_{13}[a,e]	$(\nu_{12}+2\nu_{13})$ - $2\nu_{13}$[a,f]
A (cm^{-1})	1.344794(2)	1.304274(1)	1.268209(3)	1.344351(1)	1.30434(2)
B (cm^{-1})	0.1479601(3)	0.1480398(1)	0.148120(1)	0.1478269(1)	0.14787(2)
C (cm^{-1})	0.1341163(4)	0.1345472(1)	0.134987(1)	0.1341370(1)	0.13462(2)
$10^9\delta_J$ (cm^{-1})	3.62(4)	3.57(2)	3.08(19)	3.64(1)	3.57[g]
$10^7\delta_K$ (cm^{-1})	−1.68(12)	−3.42(7)	−9.3(19)	−1.49(6)	−3.42[g]
$10^6\Delta_K$ (cm^{-1})	−5.31(1)	−13.56(2)	−18.38(4)	−5.08(2)	−14.4(2)
$10^7\Delta_{JK}$ (cm^{-1})	−2.47(2)	−2.486(6)	−2.44(2)	−2.510(5)	−2.06(15)
$10^8\Delta_J$ (cm^{-1})	2.95(2)	3.028(3)	2.98(5)	2.96(2)	2.86(5)
ν_0 (cm^{-1})		159.91102(2)	157.2524(5)	520.71037(2)	516.9868(7)
$\Delta\nu_{rms}$ (cm^{-1})	0.000372	0.000322	0.000402	0.000259	0.000458
κ	−0.977130	−0.976930	−0.976821	−0.977376	−0.977338
no. of transitions	1580	1192	538	1237	182
max K_a'	9	9	9	9	9
max J	48	54	58	54	45

[a] Uncertainty (1σ) in the last places in the fit is in parentheses. [b] Fit to pooled data for USCDs of the ν_{13} fundamental (36.5%), LSCDs from hot1 of ν_{13} (29.2%) and LSCDs from hot1 of ν_{12} (34.3%). ν_0 was not obtained in this procedure. [c] Fit to the constants in column 1 and the lines for the first hot band of ν_{13}. [d] Fit to US rotational constants for the first hot band of ν_{13} in column 2 and the lines for the second hot band of ν_{13}. [e] Fit to the constants in column 1 and the lines of the first hot band of ν_{12}. [f] Fit to the constants in column 2 and the lines for the second hot band of ν_{12}. [g] Held at the lower state value from column 2.

state rotational constants for the first and second hot bands of ν_{12}, respectively.

The A rotational constants decrease appreciably in the progression from the GS (Table 2) to the third excited state of ν_{13} (Table 4). This decrease is expected as the increase in torsional displacement around the C−C bond raises the I_a moment of inertia and thereby decreases A. In a similar manner, A decreases for the combined excited states associated with the hot bands of the ν_{12} mode. For the torsional mode the B and C rotational constants increase gradually with excitation. Another marked effect is the increase in the magnitude of the Δ_K centrifugal distortion constant with increased excitation of the ν_{13} mode. Although statistically less well determined, δ_K also appears to increase significantly in magnitude with excitation of ν_{13}. Because centrifugal distortion constants depend on force constants, increases in Δ_K and δ_K reflect weakening of force constants. In contrast to the behavior for the torsional mode, the change in A in going from the GS to the first excited state of ν_{12}, which is largely caused by out-of-plane movement of hydrogen atoms, is quite small at approximately 1/1400. The changes in the A rotational constant within the two hot bands of ν_{12} are similarly small.

Ogilvie and Cole investigated the C-type band of the ν_{12} mode with modest resolution (0.3 cm^{-1}) and analyzed the Q-branch structure in this spectrum.[35] Cole et al. made a similar analysis of the ν_{13} band, which included an investigation of two hot bands.[36] Comparisons of the earlier values of band centers, $A'' - B_{av}''$ and $A' - B_{av}'$, with the present values are in Table 5. Given the huge differences in resolution and detail available for the two studies, the constants derived in the two published studies are reasonably good. Cole and co-workers also reported values for band centers for the third and fourth hot bands as 155.1 and 152.2 cm^{-1}, as estimated from central Q branches of these bands.[36] Similar estimates by Cole et al. for the fundamental and the first two hot bands gave values that are 0.5−0.6 cm^{-1} high compared to the present values obtained from the high-resolution analysis. Our corresponding estimates were 162.65, 160.17, 157.55, 154.84, and 152.29 cm^{-1} for the central Q branches. With the exception of the last value, our estimates are lower than those of Cole et al. by 0.2−0.3 cm^{-1}. The very low intensity of the fourth hot band makes the estimate of its band center doubtful. All considered, we suggest 154.6 and 152.1 cm^{-1} as new estimates for the centers of the hot3 and hot4 bands, respectively.

TABLE 5: Comparison of Band Centers and Rotational Constants with the Literature (in cm^{-1})

	ν_0	$A'' - B_{av}''$	$A' - B_{av}'$
ν_{12} fundamental			
lit.[a]	524.5(1)	1.246(2)	1.247(2)
this work[b]	524.5739	1.2496	1.2483
ν_{13} fundamental			
lit.[c]	162.50(12)	1.245	1.2032(12)
this work[d]	162.4195	1.2496	1.2038
ν_{13} hot 1			
lit.[c]	159.98(15)	1.203	1.1653(12)
this work[d]	159.9110	1.2038	1.16298
ν_{13} hot 2			
lit.[c]	157.20(18)	1.165	1.134(12)
this work[d]	157.2424	1.1630	1.1267

[a] Reference 35. [b] Table 2. [c] Reference 36. [d] Tables 3 and 4.

Two other comparisons with the literature for transitions in the ν_{13} manifold are possible. One is with the two lowest double quantum jump transitions observed in the gas-phase Raman spectrum. We find 322.33 cm^{-1} (0→2) and 317.16 cm^{-1} (1→3) to compare with 321.6 and 316.6 cm^{-1} reported by Engeln et al. as found from band envelopes.[9] Senent computed energies (in cm^{-1}) for the torsional states with an MP2/6-31(p,d) model.[37] Values of 162.52, 322.42, and 479.48 cm^{-1} were predicted for $v = 1$, 2, and 3 to be compared with 162.42, 322.33, and 479.58 cm^{-1} from the present study. The predictions are quite good despite the level of theory. Senent also predicted centers of rotational subbands for $K_a = 3-16$. These values agree rather well within 0.13−0.56 cm^{-1} of the observed values with no discernible pattern.

3.4. Analysis of the Rotational Structure in the Weak Band Near 746 cm^{-1}. De Maré et al. observed rotational structure in the weak band near 750 cm^{-1} with a modest resolution of 0.1 cm^{-1} in the gas-phase infrared spectrum.[20] The rotational structure was attributed to Q branches of a B-type band, and the band center was placed at 749.22 cm^{-1}. Rotational constants suggested this band was from the gauche rotamer of butadiene. A reinvestigation of this band with higher resolution was a prime objective of the present work.

Preliminary studies of the spectrum of butadiene at 0, 25, and 50 °C showed that the relative intensity in the 746 cm^{-1} region increased with temperature, as would be expected for the higher energy gauche rotamer. In addition, the matrix isolation investigation summarized by the stick spectrum in Figure 1 indicated a band for the cis/gauche species in this spectral region. Figure 7 is an overall view of the high-resolution, gas-phase spectrum of this band in the infrared region at 5 Torr (160 torr m). Subband Q branches expected for a B-type band are absent. The regularly spaced lines in the P branch come from the CO_2-impurity band with an origin at 720 cm^{-1}. The overall structure of the band suggests the close spacing of lines in an A-type band and a diffuse central Q branch, degrading to higher frequency. Closer inspection of the structure confirmed this impression and led to a reassignment as a difference band of the trans rotamer.

The analysis of the rotational structure in the band at 746 cm^{-1} was facilitated by A-type LSCDs predicted in association with fitting the C-type LSCDs of the first hot band accompanying the ν_{12} fundamental for the trans rotamer. These LSCDs were essential for connecting $^{Q}R_K$ and $^{Q}P_K$ series together and assigning K_a values. To confirm and reinforce our knowledge of the LSCDs, we subsequently investigated the low frequency torsional mode directly. We now interpret the 746 cm^{-1} band as a difference band for the trans rotamer arising from $\nu_{15}(b_g)$ − $\nu_{13}(a_u)$ to give a transition with B_u symmetry, which is consistent with an A-type shape for the band. This transition is shown in the energy diagram in Figure 4.

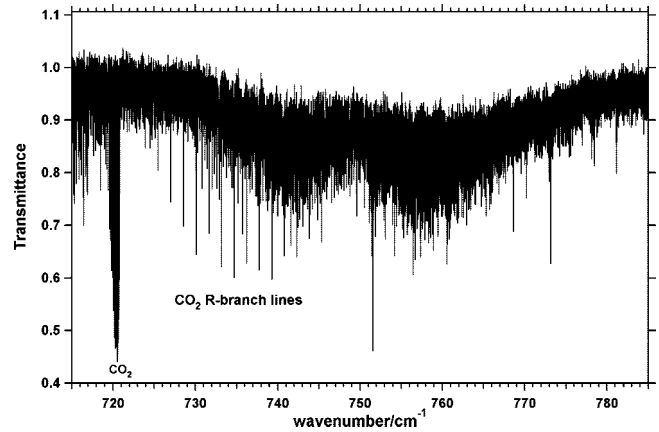

Figure 7. Overall view of the high-resolution scan of the A-type band at 746 cm^{-1} for the $\nu_{15}(b_g) - \nu_{13}(a_u)$ difference band of *s-trans*-butadiene at 5 Torr (160 Torr m).

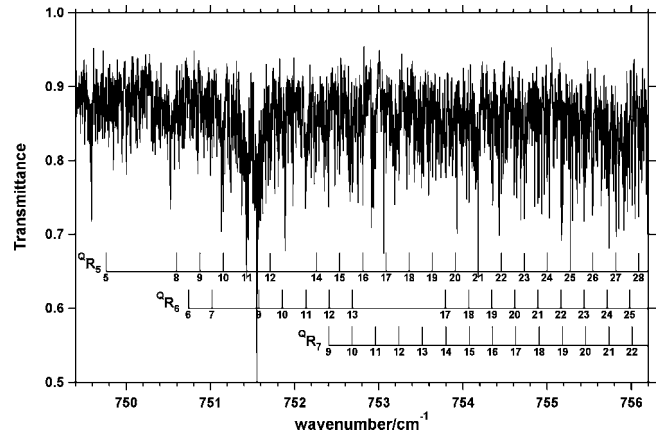

Figure 8. Details of assignments of lines in the R branch of the A-type band for the difference band of the trans rotamer.

TABLE 6: Summary of Rotational Assignments Associated with the A-Type Band of *trans*-Butadiene near 746 cm^{-1} for $\nu_{15}(b_g) - \nu_{13}(a_u)$

	no. of lines	B_{av}''/cm^{-1}	ν_0/cm^{-1}
$^{Q}P_4/^{Q}R_4$ high K_c	49	0.14111	747.498
$^{Q}P_5/^{Q}R_5$	64	0.14108	748.075
$^{Q}P_6/^{Q}R_6$	68	0.14105	748.776
$^{Q}P_7/^{Q}R_7$	76	0.14107	749.597

Although the high-resolution spectrum in the vicinity of 746 cm^{-1} is rich and complex, especially in the P branch, we were able to assign four $^{Q}R_K/^{Q}P_K$ subbands, those for $K_a = 4-7$. Other subbands with reasonable B_{av}'' values near 0.141 cm^{-1} were found, but they failed to meet the LSCD test to connect the R and P branches with the same K_a. Some of the additional bands are presumed to arise from hot bands, which should be present as for other bands in the spectrum. Figure 8 shows details of the spectrum in the R branch with combs for assignments of $^{Q}R_5-^{Q}R_7$. Table 6 summarizes the subbands assigned, and the details of the assignments are listed in Table S12 (Supporting Information).

Attempts to do an US fit for the 746 cm^{-1} band failed, presumably due to an extensive perturbation. When the ν_0 values of the subbands were fitted to a function with a single quadratic term, the overall band center was estimated to be 746.5 cm^{-1}.

This frequency compares favorably with 745.6 cm^{-1}, which is computed from ν_{13} = 162.5 cm^{-1} and ν_{15} = 908 cm^{-1}. The latter value is from the liquid-phase Raman spectrum and is likely to be lower than that for the gas phase. The perturbation affecting the observed bands must be in the US because the LS can be fit to $K_a' = 10$. The nearest binary combinations that satisfy the Jahn rule for Coriolis coupling are $2\nu_9(A_g) = 1023$ cm^{-1} and $\nu_{12} + \nu_{24} = 824$ cm^{-1} (B_g). Because the difference band arises from the first excited state of the torsion, the intensity of this band will increase with rising temperature.

To the disappointment of all who seek structural evidence for the elusive gauche rotamer, we have shown that the band near 746 cm^{-1} is merely a difference band of the abundant trans rotamer.

3.5. Search for Other Bands of the Gauche Rotamer. On the basis of finding bands at 468 and 589 cm^{-1} in matrix isolation spectra (Figure 1)[2] and on these being locations in the infrared spectrum of butadiene where relative intensities increase in going from 0 to 50 °C, the regions around 460 and 600 cm^{-1} were promising for observing rotational structure for the gauche rotamer. In addition, the 460 and 600 cm^{-1} regions are relatively far from the center at 525 cm^{-1} of the neighboring band of the trans rotamer. As a prelude to this search for evidence of the gauche rotamer, we had another strong reason to assign rotational structure for the fundamental and hot bands of the band at 525 cm^{-1}.

Our strategy for investigating the 460 cm^{-1} region was to suppress lines of the 525 cm^{-1} band in the Loomis−Wood display of the P branch in the region to be searched, which was 470−440 cm^{-1}. Lines for $^{P}P_{13}$ to $^{P}P_{29}$ subbands of the fundamental, $^{P}P_{14}$ to $^{P}P_{17}$ for the first hot band, and $^{P}P_{11}$ to $^{P}P_{18}$ for the second hot band were suppressed. For the search B_{av}'' was taken as 0.172 cm^{-1}, as found from the Cartesian coordinates for the computed structure of the gauche rotamer.[34] This value of B_{av}'' for the gauche rotamer differs substantially from the value of 0.141 cm^{-1} for the trans rotamer. Thus, subbands of the trans rotamer could not be mistaken for subbands of the gauche rotamer. B_{av}'' was varied ±0.002, and $B' - B''$ was varied from $\pm 1 \times 10^{-5}$ to $\pm 1 \times 10^{-4}$. A high-intensity scan (3.6 Torr, 115 Torr m) of the region was used in this search to improve the prospects for observing weak series from the gauche rotamer. No indications of subbands for the gauche rotamer were found.

Although subband series were not found, a couple of weak Q branches at 463.82 and 462.19 cm^{-1} are possible hints of a vibrational transition of the gauche rotamer. These frequencies cannot be explained readily by the trans rotamer. A combination band $[\nu_{13}(a_u) + \nu_{24}(b_u)]$ predicted at 463.5 cm^{-1} has B_g symmetry and thus would not be infrared active unless a perturbation is involved. A difference band $\nu_{23}(b_u) - \nu_{12}(a_u)$ for the trans rotamer at 465 cm^{-1} is an exact prediction.

A search was also conducted for subbands of the gauche rotamer in the 600 cm^{-1} region of the high-intensity spectrum (115 Torr m) but without suppressing $^{R}R_K$ subbands from the 525 cm^{-1} band. In this region the residual lines from the 525 cm^{-1} band are weaker than those in the 460 cm^{-1} region. No subbands for the gauche rotamer were found in the 600 cm^{-1} region of the spectrum.

Except for the weak Q branch features at 463.82 and 462.19 cm^{-1}, no evidence of bands for the gauche rotamer was found in the high-resolution infrared spectrum. Why is evidence for the gauche rotamer in the gas-phase infrared spectra so hard to find at room temperature? In addition to the problem of overshadowing of many bands of the gauche rotamer by those of the abundant trans rotamer, we now believe that the value of 5% reported by Saltiel et al. for the gauche content at room temperature is too high.[7] The reason for suspicion is that their value for $\Delta_r S°_{320}$ of 16.6 J/(K mol) for the trans-to-gauche conversion seems high.[7] DFT calculations with a B3LYP/aug-cc-pVTZ model gave a thermal contribution of 2.4 J/(K mol) at 298 K. When R ln 2 was added to account for the statistical weight of two gauche rotamers, $\Delta_r S°_{298}$ = 8.2 J/(K mol). This value for $\Delta_r S°_{298}$ and the accepted value for $\Delta_r H°_{298}$ predict only 2% for the gauche content at room temperature. A likely reason for the large value of the published $\Delta_r S°$ value is an error in deducing the absorption coefficients for the two rotamers during deconvolution of the UV spectra.[7]

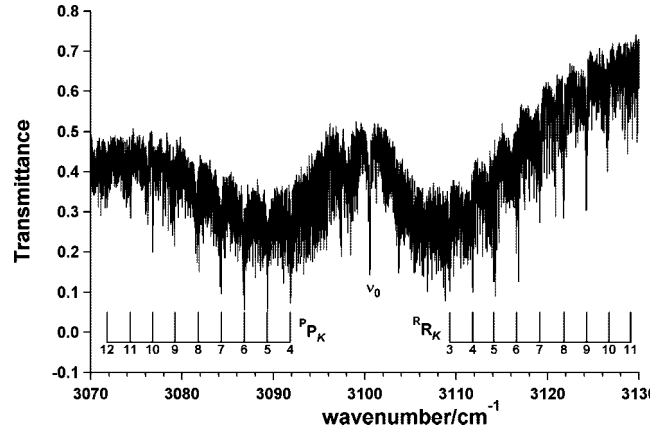

Figure 9. Overall view of the A/B-type band at 3000 cm^{-1} for the ν_{17} fundamental of the trans rotamer butadiene at 0.41 Torr (6.4 Torr m).

3.6. CH Stretching Region. Recently, Halonen, Halonen, and Nesbitt (HHN) investigated the A/B-type band near 3000 cm^{-1} for a CH stretching fundamental.[25] They did so with high-resolution (0.0016 cm^{-1}) tunable laser spectroscopy at jet beam temperature (15 K). Altogether 275 A-type and B-type transitions were assigned. The B-type component was 2.4 times more intense that the A-type component. They reported GS and US rotational constants for ν_{17} and a four-times weaker, close neighbor, designated as ν_x, which interacts with ν_{17} and also has a stronger B-type component. The US fit was compromised some (s.d. = 0.003 cm^{-1}) by interactions. Observed band centers were 3100.633 cm^{-1} for ν_{17} and 3096.143 cm^{-1} for ν_x. In addition, they identified a dark state at 3100.651 cm^{-1}, designated ν_z, which perturbs the two observed transitions.

We also investigated the CH stretching region with high-resolution (0.003 cm^{-1}) infrared spectroscopy at room temperature with a sample pressure of 0.4 Torr (6.4 Torr m). The Doppler width of 0.005 cm^{-1} for lines of butadiene at this temperature interfered with this investigation. (For the work of HHN the Doppler width at 15 K was negligibly small.) Figure 9 presents this band as recorded in the room temperature scan. Combs mark subband Q branches of the B-type component. A weak Q branch for the A-type component is designated in the band center, and dense line structure of the A-type component is evident on both sides near the band center.

The GS rotational constants obtained from our extensive investigation of many bands in the spectrum of butadiene confirmed the GS rotational constants reported by HHN, despite their redundant use of many observed lines in computing GSCDs. (Redundant use of data occurs when all CDs arising from the same upper state are computed. Many of the GSCDs found in this way are equivalent to alternate loops between observed lines.) HHN obtained 466 GSCDs from 275 lines. A

nonredundant set is only 157 GSCDs, which gives essentially the same GS constants in a rigid rotor fit. Despite the poorer resolution in the room temperature spectrum, we identified many of the lines reported by HHN but found a systematic frequency difference of about $+0.0045$ cm^{-1} for the lines in the room temperature spectrum. It is likely that HHN's use of HCl, which has strong intermolecular interactions, as a calibrant gas in the low-temperature, high-resolution spectra is the cause of this discrepancy.

Starting from HHN's very low J assignments in subbands in the low temperature spectrum, attempts were made to extend series to higher J quantum numbers in the B-type component of the band in the room temperature spectrum. However, convincing paths for these extensions could not be found in the LW displays. We attribute this failure to the degraded resolution (0.006 cm^{-1} width at half-height for sharp lines) in the spectra recorded at room temperature.

4. Summary

The weak band near 746 cm^{-1}, which increases in relative intensity with an increase in temperature, was previously assigned to the gauche rotamer of butadiene. This band has been reassigned as the difference band $\nu_{15}(b_g) - \nu_{13}(a_u) = 746$ cm^{-1} (B_u) for the trans rotamer. Careful searches in the 460 and 600 cm^{-1} regions revealed no subbands assignable to the gauche rotamer, which is predicted to have $B_{av}'' = 0.172$ cm^{-1}. Two weak Q branches at 463.82 and 462.16 cm^{-1} might be attributable to the gauche rotamer. It now seems likely that the abundance of the gauche rotamer at room temperature is only 2%, less than half the amount previously thought.

The rotational structure in the C-type band for $\nu_{12}(a_u)$ for the trans rotamer at 525.574 cm^{-1} was analyzed. The first and second hot bands, which arise from the first and second excited states of $\nu_{13}(a_u)$, the torsion, were also analyzed.

Rotational structure in the C-type band for $\nu_{13}(a_u)$, the torsional mode of the trans rotamer at 162.419 cm^{-1}, was investigated. The rotational structure for the first and second hot bands was also analyzed. LSCDs for the first and second hot bands were consistent with those found for the first and second hot bands of the 525 cm^{-1} band, thereby confirming the interpretation of the hot bands. Figure 4 is a diagram of the transitions studied.

An attempt was made to extend the published assignments for the B-type component of the band for $\nu_{17}(b_u)$ of the trans rotamer near 3000 cm^{-1}, which had previously been investigated at low temperature with high resolution in a jet-beam experiment. The large Doppler broadening in this region at room temperature interferred with this attempt.

Finding assignable rotational structure for the gauche rotamer of butadiene, from which the geometric structure could be deduced, remains an unmet challenge.

Acknowledgment. We are grateful to Dr. David Feller, who did the high-level ab initio calculations for the gauche rotamer of butadiene. Oberlin students Matthew C. Leyden, Deacon J. Nemchick, and Lynn Shen assisted in analyzing rotational structure in some of the bands. NCC was supported by several Senior Scholar Mentor grants from the Dreyfus Foundation. National Science Foundation grant 0420717 supported the purchase and technical support for the Beowulf computer cluster at Oberlin College. This research was also supported, in part, by the United States Department of Energy, Office of Basic Energy Sciences, Chemical Sciences Division. The high-resolution spectroscopy was performed at the W. R. Wiley Environmental Molecular Science Laboratory, a national scientific user facility sponsored by the Department of Energy's Office of Biological and Environmental Research located at the Pacific Northwest National Laboratory. Pacific Northwest National Laboratory is operated for the United States Department of Energy by Battelle under contract DE-AC05-76RLO 1830.

Supporting Information Available: Table S1, GSCDs from ν_{11} and ν_{12}; Table S2, assigned lines for the ν_{12} fundamental; Table S3, LSCDs from the first hot band of ν_{12}; Table S4, LSCDs from the second hot band of ν_{12}; Table S5, GSCDs from ν_{13}; Table S6, assigned lines for the ν_{13} fundamental; Table S7, pooled CDs for the upper state of ν_{13}; Table S8, assigned lines for the first hot band of ν_{13}; Table S9, assigned lines for the second hot band of ν_{13}; Table S10, assigned lines for the first hot band of ν_{12}; Table S11, assigned lines for the second hot band of ν_{12}; Table S12, assigned lines for the $\nu_{15}(b_g) - \nu_{13}(a_u)$ difference band. This material is available free of charge via the Internet at http://pubs.acs.org.

References and Notes

(1) Squillacote, M. E.; Sheridan, R. S.; Chapman, O. L; Anet, F. A. L. *J. Am. Chem. Soc.* **1979**, *101*, 3657–3659.
(2) Huber-Wälchli, P.; Günthard, Hs. H. *Spectrochim. Acta* **1981**, *37A*, 285–304.
(3) Furukawa, Y.; Takeuchi, H.; Harada, I.; Tasumi, M. *Bull. Chem. Soc. Jpn.* **1983**, *56*, 392–399.
(4) Fisher, J. J.; Michl, J. *J. Am. Chem. Soc.* **1987**, *109*, 1056–1059.
(5) Arnold, B. R.; Balaji, V.; Michl, J. *J. Am. Chem. Soc.* **1990**, *112*, 1808–1812.
(6) Choi, C. H.; Kertesz, M.; Dobrin, S.; Michl, J. *Theor. Chem. Acc.* **1999**, *102*, 196–206.
(7) Saltiel, J.; Sears, D. F., Jr.; Turek, A. M. *J. Phys. Chem. A* **2001**, *105*, 7569–7578.
(8) Mui, P. W.; Grunwald, E. *J. Am. Chem. Soc.* **1982**, *104*, 6562–6566.
(9) Engeln, R.; Consalvo, D.; Ruess, J. *Chem. Phys.* **1992**, *160*, 427–433. We evaluated the reported potential function at various angles to obtain the energies and angles reported here. Only the parameters of the potential function and the graph were supplied in the paper.
(10) Carriera, L. A. *J. Chem. Phys.* **1975**, *62*, 3851–3854.
(11) Durig, J. R.; Bucy, W. E.; Cole, A. R. H. *Can. J. Phys.* **1975**, *53*, 1832–1837.
(12) Panchenko, Yu. N.; Abramenkov, A. V.; Mochalov, V. I.; Zenkin, A. A.; Keresztury, G.; Jalsovszky, G. *J. Mol. Spectrosc.* **1983**, *99*, 288–293.
(13) Panchenko, Yu. N.; Abramenkov, A. V.; Bock, C. W. *J. Mol. Struct.* **1986**, *140*, 87–92.
(14) Karpfen, A.; Parasuk, V. *Mol. Phys.* **2004**, *102*, 819–826.
(15) Murcko, M. A.; Castejon, H.; Wiberg, K. B. *J. Phys. Chem.* **1996**, *100*, 16162–16168.
(16) Computed by Gaussian 03 C.02 with a B3LYP/aug-cc-pVTZ model.
(17) Frisch, M. J.; Trucks, G. W.; Schlegel, H. B.; Scuseria, G. E.; Robb, M. A.; Cheeseman, J. R.; Montgomery, J. A., Jr.; Vreven, T.; Kudin, K. N.; Burant, J. C.; Millam, J. M.; Iyengar, S. S.; Tomasi, J.; Barone, V.; Mennucci, B.; Cossi, M.; Scalmani, G.; Rega, N.; Petersson, G. A.; Nakatsuji, H.; Hada, M.; Ehara, M.; Toyota, K.; Fukuda, R.; Hasegawa, J.; Ishida, M.; Nakajima, T.; Honda, Y.;. Kitao, O.; Nakai, H. ; Klene, M.; Li, X.; Knox, J. E.; Hratchian, H. P.; Cross, J. B.; Adamo, C.; Jaramillo, J.; Gomperts, R.; Stratmann, R. E.; Yazyev, O.; Austin, A. J.; Cammi, R.; Pomelli, C.; Ochterski, J. W.; Ayala, P. Y.; Morokuma, K.; Voth, G. A.; Salvador, P.; Dannenberg, J. J. ; Zakrzewski, V. G. ; Dapprich, S. ; Daniels, A. D. ; Strain, S. ; Farkas, O. ; Malick, D. K.; Rabuck, A. D.; Raghavachari, K.; Foresman, J. B.; Ortiz, J. V.; Cui, Q.; Baboul, A. G.; Clifford, S.; Cioslowski, J.; Stefanov, B. B.; Liu, G.; Liashenko, A.; Piskorz, P.; Komaromi, I.; Martin, R. L.; Fox, D. J.; Keith, T.; Al-Laham, M. A.; Peng, C. Y.; Nanayakkara, A.; Challacombe, M.; Gill, P. M. W.; Johnson, B.; Chen, W.; Wong, M. W.; Gonzalez, C.; Pople, J. A. *Gaussian 03*, Revision C.02; Gaussian Inc., Wallingford, CT, 2004.
(18) Wiberg, K. B.; Rosenberg, R. E. *J. Am. Chem. Soc.* **1990**, *112*, 1509–1519.
(19) Bock, C. W.; Panchenko, Yu. N.; Krasnoshchekov, S. V.; Pupyshev, V. I. *J. Mol. Spectroscoc.* **1988**, *129*, 57–67.
(20) De Maré, G. R.; Panchenko, Yu. N.; Vander Auwera, J. *J. Phys. Chem. A* **1997**, *101*, 3998–4004.

(21) Panchenko, Y. N.; Vander Auwera, J.; Moussaoui, Y.; De Maré, G. R. *Struct. Chem.* **2003**, *14*, 337–348.
(22) Tang, W.; Bally, T. *J. Phys. Chem.* **1983**, *97*, 4365–4372.
(23) Lide, D. R. *J. Chem. Phys.* **1962**, *37*, 2074–2079.
(24) Caminati, W.; Grassi, G.; Bauder, A. *Chem. Phys. Lett.* **1988**, *148*, 13–16.
(25) Halonen, M.; Halonen, L.; Nesbitt, D. J. *J. Phys. Chem. A* **2004**, *108*, 3367–3372.
(26) Craig, N. C.; Davis, J. L.; Hanson, K. A.; Moore, M. C.; Weidenbaum, K. J.; Lock, M. *J. Phys. Chem. A* **2004**, *695*−*696*, 59–69.
(27) Maki, A.; Blake, T. A.; Sams, R. L.; Vupanovici, N.; Barber, J.; Chrysostom, E. T. H.; Masiello, T.; Nibler, J. W.; Weber, A. *J. Mol. Spectrosc.* **2001**, *210*, 240–249.
(28) Maki, A. G.; Wells, J. *J. Res. NIST* **1992**, *97*, 409–470.
(29) Rothman, L. S.; Rinsland, C. P.; Goldman, A.; Massie, S. T.; Edwards, D. P.; Flaud, J. M.; Perrin, A.; Camy-Peyret, C.; Dana, V.; Mandin, J. Y.; Schroeder, J.; McCann, A.; Gamache, R. R.; Wattson, R. B.; Yoshino, K.; Chance, K. V.; Jucks, K. W.; Brown., L. R.; Nemtchinov, V.; Varanasi, P. The HITRAN molecular spectroscopic database and HAWKS (HITRAN atmospheric workstation): 1996 edition. *JQSRT* **1998**, *60*, 665–710.
(30) Toth, R. A. *J. Mol. Spectrosc.* **1998**, *190*, 379–396.
(31) Winnewisser, B. P.; Reinstädtler, J.; Yamada, K. M. T. *J. Mol. Spectrosc.* **1989**, *136*, 12–16.
(32) Craig, N. C.; Klee, S.; Mellau, G. C.; Winnewisser, B. P.; Winnewiser, M. *J. Am. Chem. Soc.* **1996**, *100*, 15049–15055.
(33) Craig, N. C.; Abiog, O. P.; Hu, B.; Stone, S. C.; Lafferty, W. J.; Xu, L.-H. *J. Phys. Chem.* **1996**, *100*, 5310–5317.
(34) Computed by David Feller with the method described in ref 38.
(35) Ogilvie, J. F.; Cole, K. C. *J. Mol. Spectrosc.* **1970**, *35*, 332–334.
(36) Cole, A. R. H.; Green, A. A.; Osborne, G. A. *J. Mol. Spectrosc.* **1973**, *48*, 242–231.
(37) Senent, M. L. *J. Mol. Spectrosc.* **1998**, *191*, 265–275.
(38) Feller, D.; Craig, N. C.; Matlin, A. R. *J. Phys. Chem. A* **2008**, *112*, 2131–2133.

JP807677Y